AIAA JOURNAL
Vol. 36, No. 7, July 1998

Experimental and Computational Investigation of the Knoller–Betz Effect

K. D. Jones,* C. M. Dohring,† and M. F. Platzer‡
U.S. Naval Postgraduate School, Monterey, California 93943

The ability of a sinusoidally plunging airfoil to produce thrust, known as the Knoller–Betz or Katzmayr effect, is investigated experimentally and numerically. Water-tunnel experiments are performed providing flow visualization and laser Doppler velocimetry data of the unsteady wakes formed by the plunging foils. Vortical structures and time-averaged velocity profiles in the wake are compared with numerical computations from a previously developed inviscid, unsteady panel code that utilizes a nonlinear wake model. Qualitative and quantitative comparisons are excellent over a broad range of reduced frequencies and Strouhal numbers, indicating that the formation and evolution of the thrust-indicative wake structures are primarily inviscid phenomena. Results at Strouhal numbers greater than about 1.0 (based on plunge amplitude) demonstrate nonsymmetric, deflected wake patterns, where both an average thrust and an average lift are produced. These highly nonlinear wake formations are generated reproducibly, both experimentally and numerically.

Nomenclature

C_d = drag coefficient per unit span, $D/(\frac{1}{2}\rho_\infty U_\infty^2 c)$
C_t = thrust coefficient per unit span, $T/(\frac{1}{2}\rho_\infty U_\infty^2 c)$
c = chord length
D = drag per unit span
f = frequency, Hz
h = nondimensional plunge amplitude, plunge amplitude/chord length
k = reduced frequency, $\omega c/U_\infty$
Sr = Strouhal number, defined here as $\omega hc/U_\infty$
T = thrust per unit span, $-D$
t = time
U_∞ = freestream velocity
V_p = nondimensional plunge velocity, $hk = Sr$
$z(t)$ = plunge displacement, positive downward, $h\sin(\omega t)$
α = angle of attack
λ = wake wavelength (distance between vortex centers of same sign)
ρ_∞ = freestream density
ω = circular frequency, $2\pi f$

Introduction

IN independent studies in 1909 and 1912, Knoller[1] and Betz,[2] respectively, were the first ones to observe that a flapping wing creates an effective angle of attack, resulting in a normal-force vector with both lift and thrust components, as illustrated in Fig. 1. Katzmayr[3] provided the first experimental verification of the Knoller–Betz effect in 1922 when he placed a stationary airfoil into a sinusoidally oscillating wind stream and measured an average thrust. In 1924, Birnbaum[4,5] identified the conditions that lead to flutter or to thrust generation. He also suggested the use of a sinusoidally flapping (plunging) wing as an alternative to the conventional propeller.

In the following decade, the aerodynamics of plunging and pitching airfoils received much attention because of its importance for reliable flutter and gust-response analyses. However, such analyses require only the determination of the lifting forces generated by plunging or pitching airfoils, and consequently, little effort was devoted over the years to the determination of the thrust forces. Nevertheless, in 1935 von Kármán and Burgers[6] offered the first theoretical explanation of drag or thrust production based on the observed location and orientation of the wake vortices, as illustrated in Figs. 2 and 3 for drag-indicative and thrust-indicative wakes, respectively. At about the same time, Garrick[7] applied Theodorsen's inviscid, incompressible, oscillatory, flat-plate theory[8] to the determination of the thrust force and showed that plunging airfoils generate thrust over the whole frequency range, whereas pitching airfoils do so only with frequencies above a certain critical value and as a function of the pivot location. In 1939, Silverstein and Joyner[9] provided the first experimental verification of Garrick's prediction, and in 1950, Bratt[10] performed flow visualization experiments that corroborated von Kármán and Burger's observations. Of particular interest, Bratt's experimental data include several cases where a nonsymmetrical, deflected wake pattern was recorded, but no comment was made on these deflected wakes.

Birnbaum's suggestion to regard a flapping foil as an alternative (two-dimensional) propeller generated some interest over the years. Most noteworthy is Kuchemann and Weber's book,[11] in which they comment on aerodynamic propulsion in nature and observe that the propulsive efficiency of an idealized flapping wing is greater than that of a simplified propeller model because of the disadvantageous trailing vortex system generated by the propeller. In the following years, many others, e.g., Refs. 12–25, contributed to the understanding of flapping-wing aerodynamics and propulsion.

The aforementioned papers reveal a considerable lack of information on the precise characteristics of the vortical wakes generated by plunging foils. Freymuth[26] presented flow visualizations of the wakes shed by plunging and pitching airfoils, whereas Koochesfahani[27] performed both flow visualizations and quantitative laser measurements of the wake flow characteristics but limited himself to a pitching foil only. He confirmed Garrick's earlier prediction that a pitching airfoil will generate thrust only above a certain critical pitch frequency. No similar measurements seem to have been performed for plunging airfoils. Therefore, it was our objective to investigate the effect of plunge frequency and amplitude on the wake characteristics. Experimentally, dye flow visualization and laser measurements were obtained, with comparisons to linear theory and a panel code[28] using visualization software by Jones and Center.[29]

Experimental Methods

The experimental facility and methods utilized in the study are summarized here, with complete details given by Dohring.[30] The experiments were carried out in the U.S. Naval Postgraduate School

Presented as Paper 96-0078 at the AIAA 34th Aerospace Sciences Meeting, Reno, NV, Jan. 15–18, 1996; received April 4, 1996; revision received Feb. 12, 1998; accepted for publication March 11, 1998.

*Research Assistant Professor, Department of Aeronautics and Astronautics. Senior Member AIAA.
†LCDR German Navy, Graduate Student, Department of Aeronautics and Astronautics.
‡Professor, Department of Aeronautics and Astronautics. Associate Fellow AIAA.

Eidetics water tunnel (Fig. 4), a closed-circuit, continuous-flow facility with a contraction ratio of 6:1 and horizontal orientation. The test section was 38 cm wide, 51 cm high, and 150 cm long, with glass side and bottom walls permitting optical access and an open top providing simple access to the model. The side walls of the test section diverged slightly to compensate for boundary-layer growth and to maintain uniform flow velocity.

The flow velocity could be set in a range from 0 to 0.5 m/s, and it was measured by a rotating-vane flow meter at the end of the test section and digitally displayed. The freestream flow velocity in the test section at the airfoil location was measured by laser Doppler velocimetry (LDV) without the airfoil installed. The Reynolds number based on the airfoil chord length ranged from 5×10^2 for the smallest airfoil at low velocities up to 5×10^4 for the largest airfoil at high flow velocities.

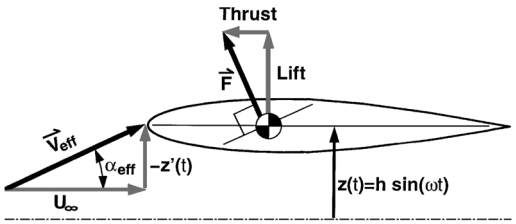

Fig. 1 Thrust and lift components of the normal force vector.

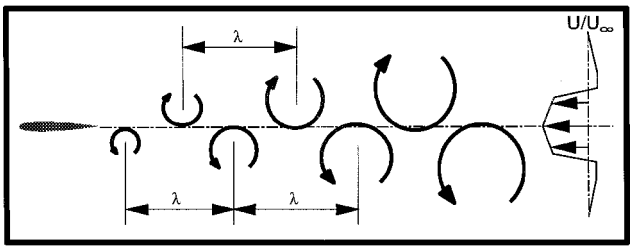

Fig. 2 Drag-indicative wake pattern.

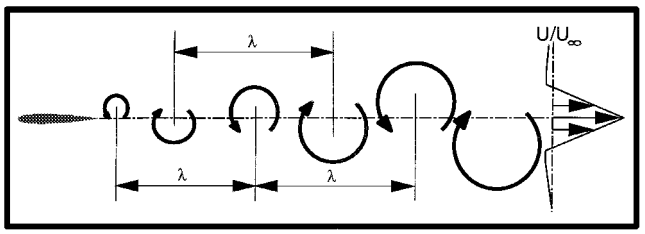

Fig. 3 Thrust-indicative wake pattern.

Water-soluble food coloring was used for flow visualization, with dye injected above and below the airfoil by two individually routed lines with adjustable horizontal and vertical position. Some experiments were carried out with only one injector upstream of the airfoil, also yielding clear wake signatures. Pressurization for the dye canisters was provided by a small compressor.

The flow visualization experiments were conducted with a 1-cm-chord-length airfoil approximating a NACA 0012. For the LDV measurements, a NACA 0012 airfoil with a chord length of 10 cm and an airfoil resembling a NACA 0015 with a 2-cm chord length were also used. All airfoils had a wing span of 37 cm and stretched across the whole test section. The airfoils were attached to a vertical shaker mounted on top of the test section. The frequency could be adjusted continuously from 5 to 60 Hz, and the amplitude could be adjusted from 0 to a maximum value dependent on the frequency. The amplitude was determined from the writing of a fixed-position needle on a paper that was attached to the moving part of the shaker. The margin of error of the amplitude measurements was approximately ± 0.25 mm.

Most measurements were conducted with a constant frequency of 5 or 10 Hz, changing the reduced frequency by adjusting the flow velocity in the tunnel. Measurements were done both at fixed reduced frequency/variable amplitude and fixed amplitude/variable reduced frequency.

The wake patterns were photographed with a 35-mm camera, and the vortical wavelength was measured from the photographs using a ruler with appropriate scale. When possible, the vortical wavelength was taken as the average of the first three fully developed vortex pairs, as illustrated in Figs. 2 and 3. The wavelength measurements relied on visual identification of the vortex centers. The margin of error in the measurements is estimated to be ± 0.8 mm, which, for the 1-cm-chord airfoil, resulted in a margin of error of ± 0.08 in the measured value of λ/c.

The LDV measurements were performed with a dual-beam, frequency-shifted, 300-mW argon ion laser with a beam separation of 50 mm, a focal length of 350 mm, and backscatter receiving

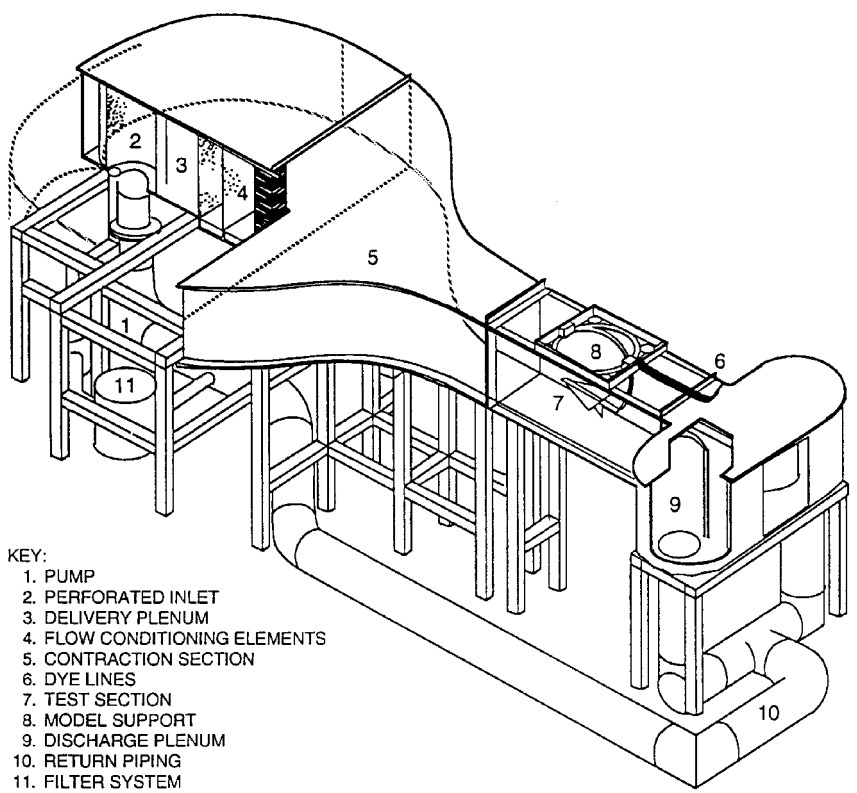

Fig. 4 Schematic of the U.S. Naval Postgraduate School Eidetics water tunnel.

optics. The Thermo Systems, Inc. (TSI), FIND software was used. The vertical distribution of the mean streamwise velocity component was measured upstream and downstream of both the stationary and the plunging airfoil. The sample size was between 400 and 1000 at an average data rate between 5 and 30 Hz; thus, a velocity averaged over many cycles was obtained. With a sample size of 1000, the maximum deviation of the LDV measurements was about 7% for unsteady flows.

Numerical Methods

Flow solutions were computed using an unsteady, potential-flow code originally developed by Teng,[28] with a graphical user interface developed by Jones and Center.[29] The basic, steady panel code follows the approach of Hess and Smith,[31] where the airfoil is approximated by a finite number of panels, each with a local, uniform, distributed source strength and all with a global, uniform, distributed vorticity strength. For n panels there are n unknown source strengths q_j and an unknown vorticity strength γ. Boundary conditions include flow tangency at the midpoint of the n panels and the Kutta condition, which postulates that the pressure on the upper and lower surfaces of the airfoil at the trailing edge must be equal.

The unsteady panel code adopts the procedure of Basu and Hancock,[32] where a wake panel is attached to the trailing edge through which vorticity is shed into the flow. The Helmholtz theorem states that the total vorticity in a flow remains constant; thus a change in circulation about the airfoil must result in the release of vorticity into the wake equal in magnitude and opposite in direction, given numerically by

$$\Delta_k(\gamma_W)_k + \Gamma_k = \Gamma_{k-1} \tag{1}$$

where Δ is the wake panel length, γ_W is the distributed vorticity strength on the wake panel, Γ is the circulation about the airfoil, k indicates the current time step, and $k-1$ indicates the previous time step.

The wake panel introduces two additional unknowns: the wake panel length and its orientation θ_k. Thus, two additional conditions must be specified for closure.

1) The wake panel is oriented in the direction of the local resultant velocity at the panel midpoint.

2) The length of the wake panel is proportional to the magnitude of the local resultant velocity at the panel midpoint and the time-step size.

The essential elements of this scheme are summarized in Fig. 5.

At the end of each time step, the vorticity contained in the wake panel is concentrated into a point vortex that is shed into the wake and convected downstream with the flow, influencing and being influenced by the other shed vortices and the airfoil. Implementation of this approach requires an iterative scheme because the velocity direction and magnitude used to define the wake panel are not initially known.

This discrete vortex wake model follows closely the nonlinear method proposed by Giesing,[33] where the computation of wake roll-up was first demonstrated. Mook et al.[34] suggested the implementation of an additional vortex-insertion method to redistribute the vorticity when stretching occurs. This approach is not used here for several reasons.

In an attempt to model vortex stretching, the vortex-insertion method redistributes wake vorticity by creating additional vortex elements when the distance between consecutively released vortices exceeds some arbitrary value. However, it seems that most of the wake stretching occurs in regions where the local vorticity is very small. Therefore, subdividing these vortex elements will have minimal effect on the overall distribution of vorticity. The subdivision of vorticity is performed only between consecutively released vortices, but in these very nonlinear wakes, the order in which the vortices are released may have little correspondence to their eventual locations in the wake.

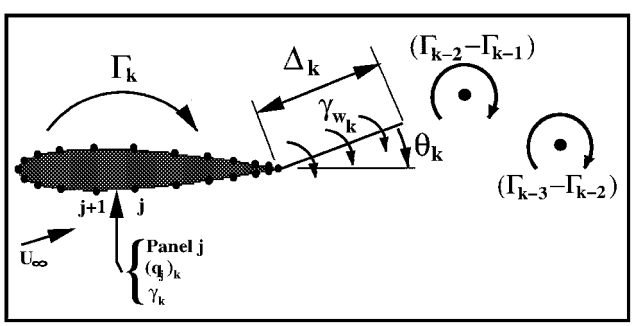

Fig. 5 Schematic of the panel code wake model.

Additionally, work by the present authors has shown that the computation of converged, i.e., time-step-independent, wake topologies for simulations that are highly nonlinear requires a large number of time steps/cycle, typically on the order of a few hundred. (The fact that the nonlinearity is lost for fewer time steps/cycle is probably something akin to the inherent smoothing of an Euler solution on a coarse grid.) In these high-frequency simulations, many cycles must be computed before the startup transients diminish. The computational expense of the wake modeling in these long computations grows rapidly because each additional time step introduces a new vortex that must be tracked. Thus, for longer simulations, the cost/step for the panel code may exceed the cost/step of an Euler or Navier–Stokes simulation, and the panel method loses its appeal. The vortex-insertion method further increases the cost of the wake modeling due to the additional vortex elements and the distance calculations that must be performed at each time step.

The unsteady panel code used here has been documented extensively (e.g., Refs. 18, 22, 25, 29, and 35–37), with unsteady force and moment comparisons to Theodorsen's and Garrick's linear theories in several of the cited references. It was shown that the panel code agrees very well with linear theory in the frequency range where wake nonlinearities are small. At high frequencies and large motion amplitudes, it was shown in Ref. 25 that the primary divergence from linear theory was due to the nonlinear wake model. Although it is difficult to quantify the accuracy of the nonlinear wake model and the resulting flowfield (except through comparative studies such as this), except in extreme cases, the computed wake topologies and surrounding flowfields were nearly independent of the number of panels used to represent the airfoil and the time-step size used. Additionally, comparisons with Navier–Stokes simulations in Ref. 22 demonstrated excellent agreement with both the wake vorticity distribution and the time-dependent lift and moment.

Time-averaged velocity profiles were computed to mimic the LDV measurements in the water tunnel. Only the streamwise velocity component was considered, and it was averaged over one or more cycles. The vortex elements were given solid-body cores that reduced singularity-induced velocity spikes in the computed profiles. The solid-body cores had essentially no effect on the shape of the wake and required no additional computational effort.

Results

The presentation of results is divided into two general sections: comparisons of wake structures (flow visualization) and comparisons of velocity profiles (LDV). First we must clarify the use of the term wake. In reference to the vortex street generated by an oscillating airfoil, the term *wake* refers to the vortical structures, implying nothing about the net drag on the airfoil. In reference to velocity profiles downstream of the airfoil, the term *wake* implies a net drag on the airfoil (Fig. 2), whereas the term *jet* implies a net thrust (Fig. 3).

Flow Visualization

In viscous fluids, stationary airfoils and airfoils plunging sinusoidally with low V_p generate drag. (Note that V_p, as defined in the Nomenclature, is hk and represents the maximum nondimensional plunge velocity. If the dimensional plunge amplitude is used as the length scale in the Strouhal number, then V_p and Sr are equivalent.) As V_p is increased, the drag is reduced, and eventually thrust is produced. The vortex streets indicative of drag-producing, neutral, and thrust-producing cases are shown schematically and experimentally in Figs. 6–8, respectively. Experimental results for the three cases are for the 1-cm airfoil oscillating at $k = 3.6$ and $h = 0.08$ ($V_p = 0.29$), $k = 5.7$ and $h = 0.08$ ($V_p = 0.46$), and $k = 3.0$ and $h = 0.20$ ($V_p = 0.60$), respectively.

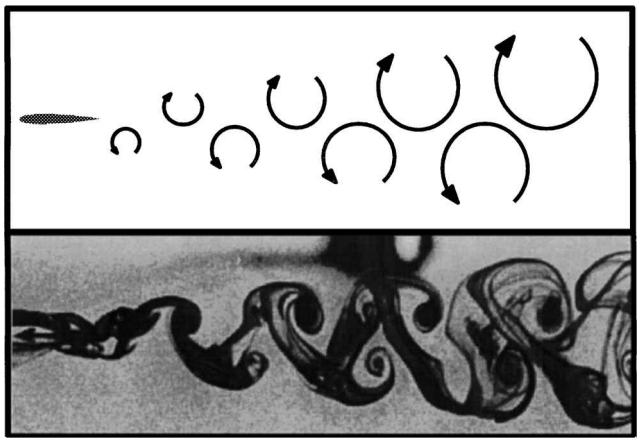

Fig. 6 Vortex street indicative of drag production (V_p = 0.29).

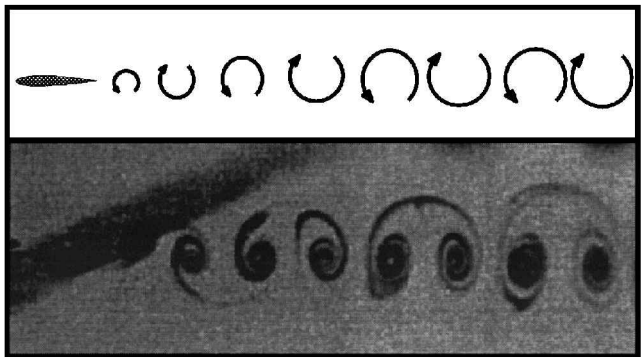

Fig. 7 Vortex street indicative of zero drag (V_p = 0.46).

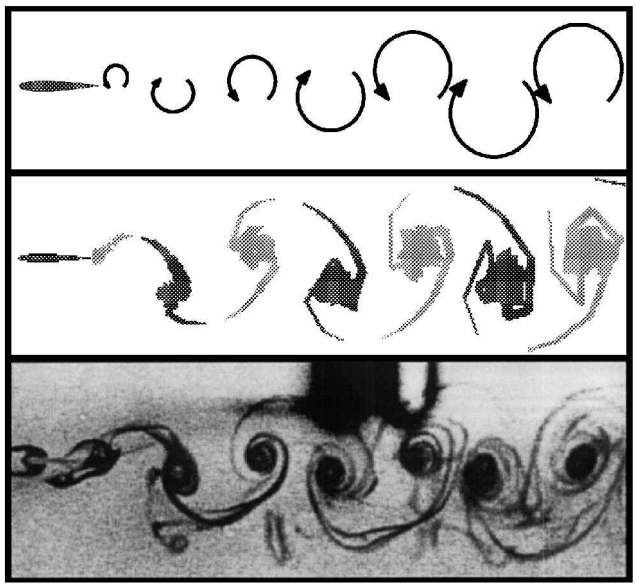

Fig. 8 Vortex street indicative of thrust production (V_p = 0.60).

For large V_p, a deflected or dual-mode vortex street is generated, as shown in Fig. 9. In this case, $k = 12.3$ and $h = 0.12$, resulting in $V_p = 1.5$. Here, in addition to a net thrust, a net lift is observed according to the deflection of the vortex street and the computed, time-averaged lift coefficient.

In Figs. 6–9, the upper image is a schematic illustrating the rotational orientation of the eddies, and the lower image is a photo from the water tunnel. In Figs. 8 and 9, the central image is a snapshot of the wake structures computed by the panel code. The potential-flow code predicts zero drag for a stationary airfoil and thrust for an airfoil plunging at any finite frequency. Consequently, there are no numerical solutions with wake structures comparable to those in Figs. 6 and 7.

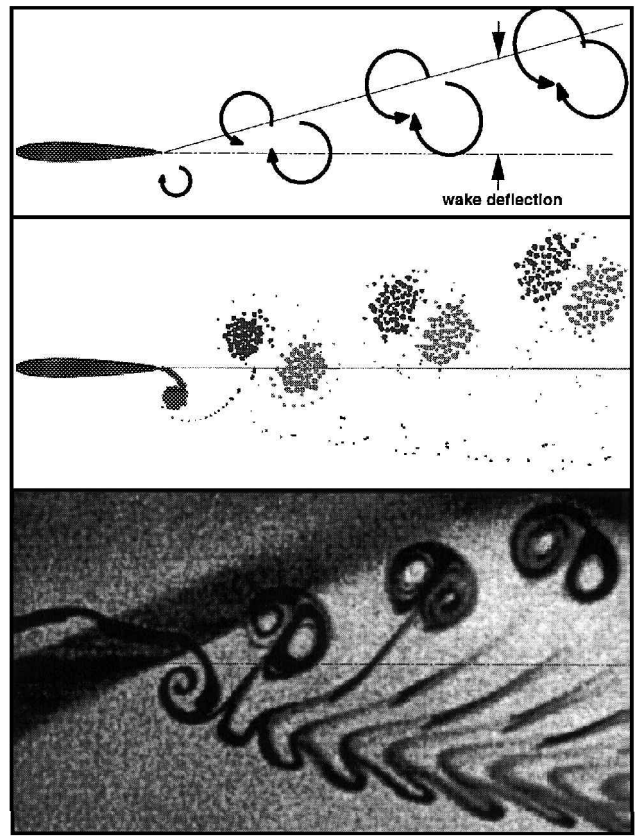

Fig. 9 Dual-mode vortex street indicative of thrust and lift (V_p = 1.50).

Numerically, the mode (vortex street deflected up or down) is determined by the initial conditions and appears to be fixed throughout the simulation. However, in the water tunnel, the vortex street seemed to alternate between modes somewhat randomly, suggesting that relatively small disturbances may trigger the switch. This is discussed in more detail in the next section.

Qualitative and quantitative comparisons of the wake structures are made by comparing photographs of the water-tunnel experiments with the digital images from the panel code, such as those shown in Figs. 8 and 9. The qualitative agreement demonstrated in Figs. 8 and 9 is astonishing. The fact that inviscid theory so accurately captures these highly nonlinear, deflected wakes suggests that the evolution of the vortical structures is essentially an inviscid phenomenon.

Quantitative comparisons between experiment and computation are more difficult. The wake wavelength, defined here as the distance between vortices of like rotation (as indicated in Figs. 2 and 3), is estimated by predicting the location of the vortex centers in the experimental and numerical images. Note that both the experimental and numerical data for this are based on observations of vortex positions, and consequently, the margin of error is not well defined. For the experimental data, it is estimated to be on the order of $\pm 0.08/c$, and this is probably appropriate for the numerical data as well.

The measured wake wavelengths are plotted in Fig. 10 as a function of the plunge amplitude for $k = 3.00$, 6.83, and 12.32. The curves from the panel code approximately extrapolate to the wavelengths predicted by linear theory ($\lambda = 2\pi/k$), $\lambda = 2.09$, 0.92, and 0.51, respectively, as the plunge amplitude approaches zero. The agreement between linear theory and the panel code is notably worse at low frequencies. The wake roll-up is minimal in these cases, and the determination of the vortex centers becomes difficult. As expected, due to profile drag, the experimentally measured wavelengths underpredict linear theory at low frequencies and plunge amplitudes but agree well with the panel code at higher frequencies and amplitudes.

The panel code predicts a thrust coefficient that is roughly proportional to the square of V_p. For all nonzero V_p, the panel code predicts a positive thrust and, hence, a wake wavelength larger than

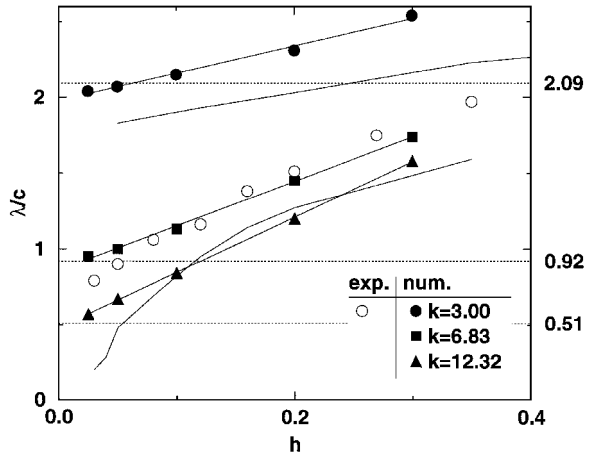

Fig. 10 Observed wake wavelengths vs h/c.

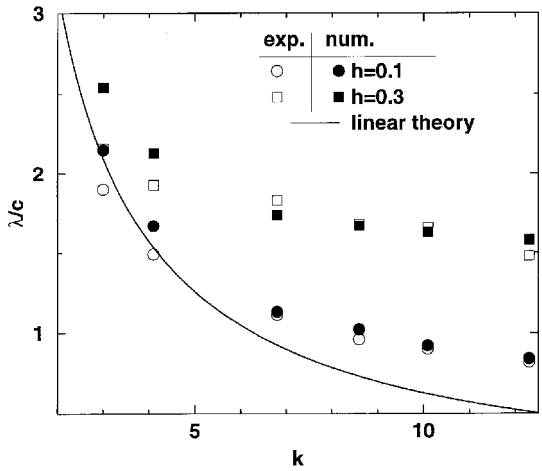

Fig. 11 Observed wake wavelengths vs k.

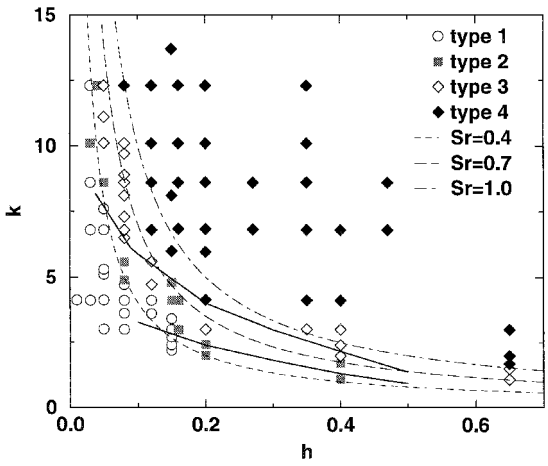

Fig. 12 Wake classification based on observed vortex positions.

that predicted by linear theory. In Fig. 11, the wake wavelength is plotted as a function of k. Note that the panel code results approach linear theory as hk approaches zero. However, the agreement between experiment and the panel code is better as hk increases, and for small hk the experimentally measured wavelengths are shorter than those predicted by linear theory; i.e., drag, not thrust, is produced. This is verified by the experimental wake pattern shown in Fig. 6, which resembles the characteristic von Kármán vortex street, signifying the generation of drag by a cylinder in viscous flow.

In Fig. 12, the experimentally photographed wakes are classified according to the observed vortex positions: Type 1 indicates drag production (as shown in Fig. 6); type 3 indicates thrust production (as shown in Fig. 8), type 2 being the dividing line between types

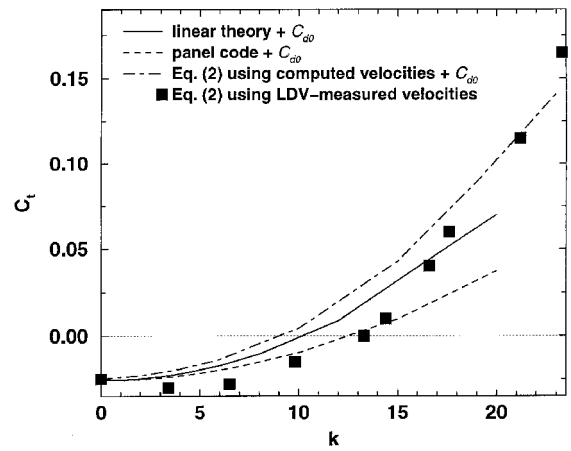

Fig. 13 Inaccuracy of C_t predictions using Eq. (2).

1 and 3, where neither drag nor thrust is generated (as shown in Fig. 7); and type 4 indicates that thrust and lift are produced (as shown in Fig. 9). Lines of constant Strouhal number are included, demonstrating the approximate dependence of the experimental data on the Strouhal number. Triantafyllou et al.[19] show a similar plot, classifying the experimental results of Ohashi and Ishikawa[38] and Kadlec and Davis[39] in the same fashion. The two solid lines in Fig. 12 are taken from Ref. 19 and are curvefit boundaries between the type 1, 2, and 3 wake topologies based on the experimental data of Refs. 38 and 39.

The type 4, deflected-wake topology (as shown in Fig. 9) was apparently not observed in any of the cited references other than Ref. 10. Although Ref. 10 includes several figures that clearly record similar deflected wakes, as previously mentioned, no remarks were made in Ref. 10 regarding them. In the present study, they were duplicated experimentally and numerically and were found to be highly reproducible.

Note that these classifications are based purely on visual observations of the unsteady vortex structures. More quantitative experimental measurements, as well as the panel code, suggest that these classifications are fairly conservative, with thrust generation occurring at Strouhal numbers as low as 0.1.

LDV Measurements

The thrust coefficient is normally computed by the panel code by integrating the streamwise component of the surface pressure coefficient. The accuracy of this approach is well documented in Ref. 25. Unfortunately, thrust measurements in the water tunnel are not so straightforward.

In many experimental investigations, the drag or thrust generated by a body is predicted by measuring the momentum deficit or surplus downstream of the body. Usually the assumptions are made that at the cross section where velocities are measured the flow is parallel, the pressure is freestream, and the time-fluctuating quantities are small, reducing the momentum integral to the simplified equation

$$T = \rho_\infty \int_{-\infty}^{+\infty} U(y)[U(y) - U_\infty]\,\mathrm{d}y \qquad (2)$$

If the velocity measurements are made sufficiently far downstream of the airfoil, such that the wake eddies are essentially diffused, then Eq. (2) yields reasonable results, but if the measurements are made in a region where the eddies are still coherent and energetic, then the assumptions will not hold. For example, Koochesfahani[27] used LDV to measure time-averaged velocity profiles downstream of a NACA 0012 airfoil pitching sinusoidally about its quarter-chord between ± 2 deg, and he applied the simplified momentum integral, Eq. (2), to compute the thrust coefficient. His measurements are compared with linear theory and the panel code in Fig. 13. Panel code thrust coefficients computed using both the conventional surface pressure integration approach and the simplified momentum integration approach with computed time-averaged velocity profiles are included. The linear theory and panel code results, all of

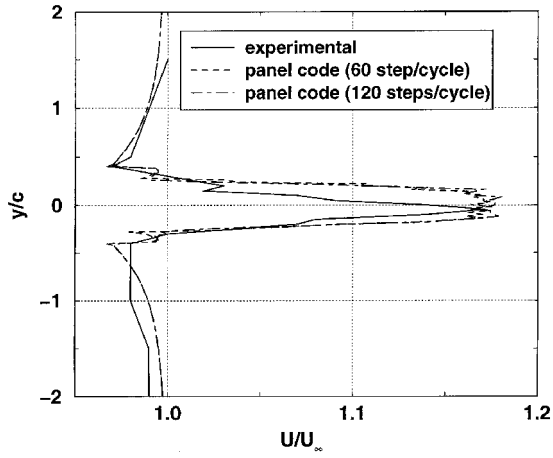

Fig. 14 Comparison of time-averaged velocity profiles for $V_p = 0.37$.

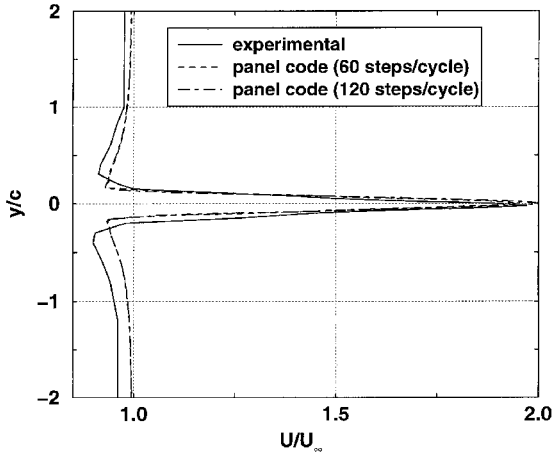

Fig. 15 Comparison of time-averaged velocity profiles for $V_p = 0.60$.

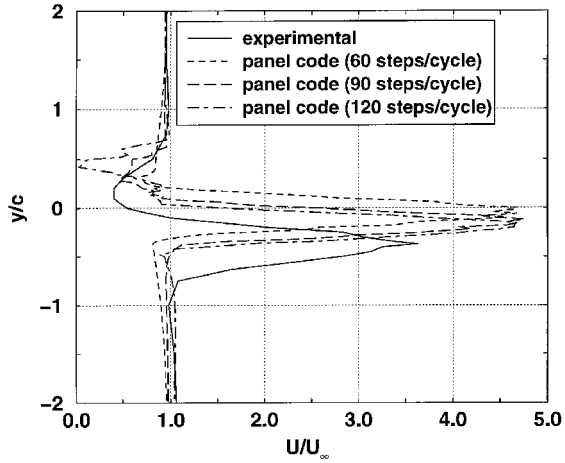

Fig. 16 Comparison of time-averaged velocity profiles for $V_p = 2.30$.

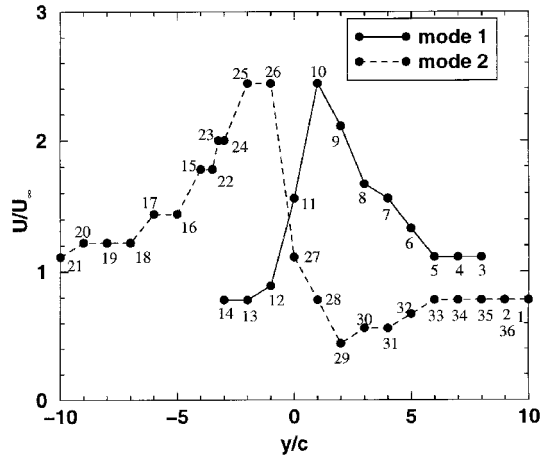

Fig. 17 Random dual-mode behavior evident in the LDV measurements.

which are inviscid, have been shifted by Koochesfahani's measured zero-frequency drag to approximate the effect of profile drag.

The panel code underpredicts linear theory over the full frequency range, as expected due to the wake nonlinearities present in the panel solution, but using Eq. (2) with either LDV-measured or -computed, time-averaged velocity profiles, a thrust greatly exceeding both the panel code and linear theory is predicted. Although the use of Eq. (2) for steady and low-frequency motions may produce reliable results, clearly at these high frequencies with extremely energetic and coherent wake structures, it does not.

Because of the preceding argument, thrust predictions are not made from the present experimental results. Instead, direct comparisons of the velocity profiles measured by LDV in the water tunnel and computed by the panel code are made. As previously mentioned, only the streamwise velocity component is measured by LDV, and between 400 and 1000 samples are used for the time-averaged values. With a sample size of 1000, the maximum deviation of the measurements was about 7% for unsteady flows.

Nondimensional velocity profiles computed by the panel code and measured in the water tunnel are compared in Figs. 14–16 for cases with $k = 4.2$ and $h = 0.088$ ($V_p = 0.37$), $k = 15.0$ and $h = 0.04$ ($V_p = 0.60$), and $k = 26.1$ and $h = 0.088$ ($V_p = 2.30$), respectively. In Figs. 14 and 16, the profile is measured $0.75c$ downstream of the trailing edge of the 2-cm NACA 0015 airfoil oscillating at 10 Hz with freestream velocities of 0.300 and 0.048 m/s, respectively. In Fig. 15, the profile is measured $0.4c$ downstream of the trailing edge of the 10-cm NACA 0012 airfoil oscillating at 5 Hz with a freestream velocity of 0.210 m/s. Note that the accuracy of the experimental oscillation amplitudes is ± 0.25 mm, and thus the amplitude error as a percentage of the chord length for the 2-cm airfoil tests is considerably larger than for the 10-cm airfoil.

The agreement between computational and experimental velocity profiles is quite good for the lower values of V_p, indicating that thrust generation in this regime is essentially an inviscid phenomenon. As V_p increases, the profiles become asymmetric along with the deflected wake, but the asymmetry in the experimentally measured profiles is more pronounced than the numerically predicted profiles, indicating that flow physics not considered in the potential-flow code is becoming dominant.

Panel code results are presented in Figs. 14–16 for several time-step sizes, providing some measure of the numerical accuracy of the approach. In the two lower-frequency cases, the numerical results are essentially time step independent, but in the third case, with a very pronounced deflected wake, the asymmetry of the computed wake becomes more pronounced as the time step becomes finer.

It was previously mentioned that the experimental wake patterns may alternate somewhat arbitrarily between modes (vortex street deflected up or down). The switching between modes did not appear to be a periodic feature, and it was never predicted in the numerical simulations. The panel code typically could not be run through more than 30 or 40 cycles in cases where deflected wakes occurred, but the wake shape and the time history of the lift and drag seemed to approach a limit asymptotically, suggesting that the solution would not switch modes. However, the fact that the experimental wakes switched somewhat randomly between modes indicates that a relatively small disturbance may be sufficient to initiate the change.

The switch between the two modes is demonstrated in Fig. 17, where a sequence of LDV measurements is plotted. The number next to each data point indicates the order in which the data were obtained. There are two discontinuities in the graph between points 2 and 3 and points 14 and 15. The wake structure has obviously switched between the two modes. This was confirmed in other experiments by recording flow visualization and LDV data simultaneously. These data cover two sweeps across the flowfield, and each data point is a time average of LDV data obtained over many cycles. The complete set of data spans thousands of cycles.

Conclusions

Water-tunnel experiments and numerical simulations were performed to investigate the generation and evolution of wake structures behind flapping wings. Experimental techniques for flow-visualization and LDV velocity-profile measurements were detailed, and an unsteady panel method incorporating a nonlinear, deforming wake model was described.

Two-color, dye-injection, flow-visualization data were shown to agree very well with the inviscid panel code predictions over a wide range of frequencies and Strouhal numbers, suggesting that the evolution of these unsteady wake structures is essentially an inviscid phenomenon.

At Strouhal numbers greater than 1, dual-mode, deflected wake patterns were found both experimentally and numerically. Numerically, the mode (deflected up or down) seemed to be determined solely by the initial conditions, and reasonably small time steps were required to model this highly nonlinear feature. Experimentally, the wakes were observed to randomly (not periodically) alternate between modes, suggesting that relatively small disturbances may be sufficient to trigger the switch.

It was shown that thrust predictions based on the simplified momentum integral for such energetic wakes yield very poor accuracy. Consequently, direct thrust comparisons were not made, but, instead, the time-averaged velocity profiles measured experimentally by LDV and computed by the panel code were compared. The agreement was found to be very good over a broad range of Strouhal numbers. At very low Strouhal numbers ($\approx$0.3) drag, not thrust, was generated, due to viscous effects, resulting in a poor agreement with the inviscid panel method. At very high Strouhal numbers ($\approx$2), where the wake deflection was rather prominent, the experimental velocity profiles showed more asymmetry than the panel code, indicating that viscous effects (probably flow separation in this case) may again be influential in the wake formation and evolution.

Acknowledgments

This investigation was partially supported by the U.S. Naval Postgraduate School, National Research Council Fellowship Program, and the Office of Naval Research, Project Officers P. Majumdar and E. Rood.

References

[1]Knoller, R., "Die Gesetze des Luftwiderstandes," *Flug- und Motortechnik (Wien)*, Vol. 3, No. 21, 1909, pp. 1–7.

[2]Betz, A., "Ein Beitrag zur Erklärung des Segelfluges," *Zeitschrift für Flugtechnik und Motorluftschiffahrt*, Vol. 3, Jan. 1912, pp. 269–272.

[3]Katzmayr, R., "Effect of Periodic Changes of Angle of Attack on Behavior of Airfoils," NACA Rept. 147, Oct. 1922 (translated from *Zeitschrift für Flugtechnik und Motorluftschiffahrt*, March 31, 1922, pp. 80–82, and April 13, 1922, pp. 95–101).

[4]Birnbaum, W., "Das ebene Problem des schlagenden Flügels," *Zeitschrift für Angewandte Mathematik und Mechanik*, Vol. 4, No. 4, 1924, pp. 277–292.

[5]Birnbaum, W., "Der Schlagflügelpropeller und die kleinen Schwingungen elastisch befestigter Tragflügel," *Zeitschrift für Flugtechnik und Motorluftschiffahrt*, Vol. 15, Nov.–Dec. 1924, pp. 128–134.

[6]von Kármán, T., and Burgers, J. M., "General Aerodynamic Theory—Perfect Fluids," *Aerodynamic Theory*, edited by W. F. Durand, Division E, Vol. 2, Julius–Springer, Berlin, 1943, p. 308.

[7]Garrick, I. E., "Propulsion of a Flapping and Oscillating Airfoil," NACA Rept. 567, 1936.

[8]Theodorsen, T., "General Theory of Aerodynamic Instability and the Mechanism of Flutter," NACA Rept. 496, 1935.

[9]Silverstein, A., and Joyner, U. T., "Experimental Verification of the Theory of Oscillating Airfoils," NACA Rept. 673, 1939.

[10]Bratt, J. B., "Flow Patterns in the Wake of an Oscillating Airfoil," Aeronautical Research Council, R&M 2773, March 1950.

[11]Kuchemann, D., and Weber, J., "Aerodynamic Propulsion in Nature," *Aerodynamics of Propulsion*, McGraw–Hill, New York, 1953, pp. 248–260.

[12]Schmidt, W., "Der Wellpropeller, ein neuer Antrieb für Wasser-, Land-, und Luftfahrzeuge," *Zeitschrift für Flugwissenschaften*, Vol. 13, No. 12, 1965, pp. 472–479.

[13]Bosch, H., "Interfering Airfoils in Two-Dimensional Unsteady Incompressible Flow," CP-227, AGARD, Paper 7, Sept. 1977.

[14]McKinney, W., and DeLaurier, J., "The Wingmill: An Oscillating Wing Windmill," *Journal of Energy*, Vol. 5, No. 2, 1981, pp. 109–115.

[15]DeLaurier, J. D., and Harris, J. M., "Experimental Study of Oscillating-Wing Propulsion," *Journal of Aircraft*, Vol. 19, No. 5, 1982, pp. 368–373.

[16]Liu, P., "Three-Dimensional Oscillating Foil Propulsion," Masters Engineering Thesis, Dept. of Mechanical Engineering, Memorial Univ. of Newfoundland, St. John's, NF, Canada, March 1991.

[17]Send, W., "The Mean Power of Forces and Moments in Unsteady Aerodynamics," *Zeitschrift für Angewandte Mathematik und Mechanik*, Vol. 72, No. 2, 1992, pp. 113–132.

[18]Platzer, M. F., Neace, K. S., and Pang, C. K., "Aerodynamic Analysis of Flapping Wing Propulsion," AIAA Paper 93-0484, Jan. 1993.

[19]Triantafyllou, G. S., Triantafyllou, M. S., and Grosenbaugh, M. A., "Optimal Thrust Development in Oscillating Foils with Application to Fish Propulsion," *Journal of Fluids and Structures*, Vol. 7, 1993, pp. 205–224.

[20]Hall, K. C., and Hall, S. R., "Minimum Induced Power Requirements for Flapping Flight," *Journal of Fluid Mechanics*, Vol. 323, Sept. 1996, pp. 285–315.

[21]Hall, K. C., Pigott, S. A., and Hall, S. R., "Power Requirements for Large-Amplitude Flapping Flight," AIAA Paper 97-0827, Jan. 1997.

[22]Tuncer, I. H., and Platzer, M. F., "Thrust Generation Due to Airfoil Flapping," *AIAA Journal*, Vol. 34, No. 2, 1996, pp. 324–331.

[23]Streitlien, K., Triantafyllou, G. S., and Triantafyllou, M. S., "Efficient Foil Propulsion Through Vortex Control," *AIAA Journal*, Vol. 34, No. 11, 1996, pp. 2315–2319.

[24]Karkehabadi, R., and Mook, D. T., "Wing in Heaving Oscillatory Motion," *Journal of Aircraft*, Vol. 33, No. 5, 1996, pp. 913–918.

[25]Jones, K. D., and Platzer, M. F., "Numerical Computation of Flapping-Wing Propulsion and Power Extraction," AIAA Paper 97-0826, Jan. 1997.

[26]Freymuth, P., "Propulsive Vortical Signatures of Plunging and Pitching Airfoils," *AIAA Journal*, Vol. 26, No. 7, 1988, pp. 881–883.

[27]Koochesfahani, M. M., "Vortical Patterns in the Wake of an Oscillating Airfoil," *AIAA Journal*, Vol. 27, No. 9, 1989, pp. 1200–1205.

[28]Teng, N. H., "The Development of a Computer Code for the Numerical Solution of Unsteady, Inviscid and Incompressible Flow over an Airfoil," M.S. Thesis, Dept. of Aeronautics and Astronautics, U.S. Naval Postgraduate School, Monterey, CA, June 1987.

[29]Jones, K. D., and Center, K. B., "Numerical Wake Visualization for Airfoils Undergoing Forced and Aeroelastic Motions," AIAA Paper 96-0055, Jan. 1996.

[30]Dohring, C. M., "Experimental Analysis of the Wake of an Oscillating Airfoil," M.S. Thesis, Dept. of Aeronautics and Astronautics, U.S. Naval Postgraduate School, Monterey, CA, June 1996.

[31]Hess, J. L., and Smith, A. M. O., "Calculation of Potential Flow About Arbitrary Bodies," *Progress in Aeronautical Sciences*, Vol. 8, Pergamon, Oxford, England, UK, 1966, pp. 1–138.

[32]Basu, B. C., and Hancock, G. J., "The Unsteady Motion of a Two-Dimensional Aerofoil in Incompressible Inviscid Flow," *Journal of Fluid Mechanics*, Vol. 87, 1978, pp. 159–168.

[33]Giesing, J. P., "Nonlinear Two-Dimensional Unsteady Potential Flow with Lift," *Journal of Aircraft*, Vol. 5, No. 2, 1968, pp. 135–143.

[34]Mook, D. T., Roy, S., Choksi, G., and Dong, B., "Numerical Simulation of the Unsteady Wake Behind an Airfoil," *Journal of Aircraft*, Vol. 26, No. 6, 1989, pp. 509–514.

[35]Neace, K. S., "A Computational and Experimental Investigation of the Propulsive and Lifting Characteristics of Oscillating Airfoils and Airfoil Combinations in Incompressible Flow," M.S. Thesis, Dept. of Aeronautics and Astronautics, U.S. Naval Postgraduate School, Monterey, CA, Sept. 1992.

[36]Riester, P. J., "A Computational and Experimental Investigation of Incompressible Oscillatory Airfoil Flow and Flutter Problems," M.S. Thesis, Dept. of Aeronautics and Astronautics, U.S. Naval Postgraduate School, Monterey, CA, June 1993.

[37]Turner, M., "A Computational Investigation of Wake-Induced Airfoil Flutter in Incompressible Flow and Active Flutter Control," M.S. Thesis, Dept. of Aeronautics and Astronautics, U.S. Naval Postgraduate School, Monterey, CA, March 1994.

[38]Ohashi, H., and Ishikawa, N., "Visualization Study of a Flow Near the Trailing Edge of an Oscillating Airfoil," *Bulletin of the Japanese Society of Mechanical Engineers*, Vol. 15, 1972, pp. 840–845.

[39]Kadlec, R. A., and Davis, S. S., "Visualization of Quasiperiodic Flows," *AIAA Journal*, Vol. 17, 1979, pp. 1164–1169.

F. W. Chambers
Associate Editor